catalysts

MDPI

Article

Pd+Al_2O_3-Supported Ni-Co Bimetallic Catalyst for H_2 Production through Dry Reforming of Methane: Effect of Carbon Deposition over Active Sites

Anis H. Fakeeha [1], Dharmesh M. Vadodariya [2], Mohammed F. Alotibi [3,*], Jehad K. Abu-Dahrieh [4,*], Ahmed A. Ibrahim [1], Ahmed E. Abasaeed [1], Naif Alarifi [3], Rawesh Kumar [2] and Ahmed S. Al-Fatesh [1,*]

[1] Chemical Engineering Department, College of Engineering, King Saud University, P.O. Box 800, Riyadh 11421, Saudi Arabia; anishf@ksu.edu.sa (A.H.F.); aididwthts2011@gmail.com (A.A.I.); abasaeed@ksu.edu.sa (A.E.A.)
[2] Department of Chemistry, Indus University, Ahmedabad 382115, India; dharmikpatel0111@gmail.com (D.M.V.); kr.rawesh@gmail.com (R.K.)
[3] Institute of Refining and Petrochemicals Technologies, King Abdulaziz City for Science and Technology (KACST), P.O. Box 6086, Riyadh 11442, Saudi Arabia; naalarifi@kacst.edu.sa
[4] School of Chemistry and Chemical Engineering, Queen's University Belfast, Belfast BT9 5AG, UK
* Correspondence: mfalotaibi@kacst.edu.sa (M.F.A.); j.abudahrieh@qub.ac.uk (J.K.A.-D.); aalfatesh@ksu.edu.sa (A.S.A.-F.); Tel.: +44-7988-769391 (J.K.A.-D.); +966-11-467-6859 (A.S.A.-F.)

Abstract: Dry reforming of methane (DRM) is gaining global attention due to its capacity to convert two greenhouse gases together. It proceeds through CH_4 decomposition over active sites (into CH_{4-x}) followed by CH_{4-x} oxidation by CO_2 (into syngas). Furthermore, CH_{4-x} oligomerization into coke cannot be neglected. Herein, xNi(5−x)Co/Pd+Al_2O_3 (x = 5, 3.75, 2.5, 1.25, 0) catalysts are prepared, investigated for DRM, and characterized with X-ray diffraction, UV-Vis, transmission electron microscopy, temperature-programmed reduction/desorption techniques, and thermogravimetry. Fine-tuning among stable active sites, graphitic carbon deposits, and catalytic activity is noticed. The total reducibility and basicity are found to decrease upon increasing the Co proportion up to 2.5 wt% in the Ni-Co bimetallic Pd+Al_2O_3-supported catalyst. The active sites derived from strong metal–support interaction species ($NiAl_2O_x$ or dispersed CoO_x) are found to be promising in higher levels of activity. However, activity is, again, limited by graphitic carbon which is increased with an increasing Co proportion in the Ni-Co bimetallic Pd+Al_2O_3-supported catalyst. The incorporation of 1.25 wt% Co along with 3.75 wt% Ni over Pd+Al_2O_3 results in the generation of fewer such active sites, extensive oxidizable carbon deposits, and inferior catalytic activity compared to 5Ni/Pd+Al_2O_3. The 2.5Ni2.5Co/Pd+Al_2O_3 catalyst has lower crystallinity, a relatively lower coke deposit (than the 3.75Ni1.25Co/Pd+Al_2O_3 catalyst), and a higher number of stable active sites. It attains a 54–51% H_2 yield in 430 min TOS and 0.87 H_2/CO (similar to 5Ni/Pd+Al_2O_3)

Keywords: graphitic coke; DRM; Ni–Co bimetallic; Pd+Al_2O_3 support; $NiAl_2O_x$

Citation: Fakeeha, A.H.; Vadodariya, D.M.; Alotibi, M.F.; Abu-Dahrieh, J.K.; Ibrahim, A.A.; Abasaeed, A.E.; Alarifi, N.; Kumar, R.; Al-Fatesh, A.S. Pd+Al_2O_3-Supported Ni-Co Bimetallic Catalyst for H_2 Production through Dry Reforming of Methane: Effect of Carbon Deposition over Active Sites. *Catalysts* **2023**, *13*, 1374. https://doi.org/10.3390/catal13101374

Academic Editor: José Antonio Calles

Received: 20 September 2023
Revised: 8 October 2023
Accepted: 14 October 2023
Published: 18 October 2023

1. Introduction

Global warming is now not only limited to the melting of glaciers and the rise of sea levels but it has become the major cause of tremendous disturbances in seasonal cycles across the globe. The main cause of this issue is attributed to greenhouse gases like CO_2 and CH_4. The catalytic conversion of both CH_4 and CO_2 into syngas (CO+H_2), popularly known as dry reforming of methane (DRM), has brought major attention to the scientific community. More importantly, the product syngas has synthetic utility in industry and may be a hydrogen source to be exploited in order to achieve future clean energy goals. The catalytic conversion of CH_4 and CO_2 into syngas is summarized into two sequential steps. The first step is the decomposition of CH_4 into CH_{4-x} and (x/2)H_2 [1]. The second step comprises two routes related to CH_{4-x} oligomerization (into coke) and CH_{4-x} oxidation

by CO_2 (into H_2 and CO). Coke formation over the catalyst surface seriously affects the H_2 and CO yield. Additionally, the deposition of inert coke-like graphite over catalytic active sites may deactivate the catalyst permanently.

Various noble metals, Co, and Ni dispersed over a proper thermally sustainable support are found to be catalytically active for DRM reactions [2]. The methane dissociation energy over Ni was, again, less than that over Pt and Pd [3]. Comparing the activation barrier for CO_2 and CH_4 dissociation, the catalytic activity of Ni was found to be better than that of noble metals [4]; the interaction energy of CH_4 over Ni was found to be 18 kcal/mol whereas over Co, it was 0.7 kcal/mol [5]. After interaction with CH_4, the electronic configuration of metallic Co is not changed, but the electronic configuration of Ni is changed to $s^{0.54}d^{9.42}$ (concerning d^8s^2 electronic configuration of metallic Ni) [6]. Cobalt addition increased the active oxygen amount/high oxygen affinity and coke resistance [6–8]. The Co^{+2}/Co^{3+} ratio over the catalyst's surface also nurtures oxygen vacancy. The vacancy induces abundant unsaturated coordination sites and high-energy dangling bonds. These vacancies are prominent sites for CO_2 adsorption and dissociation [9,10]. Huang et al. identified adsorption structures of species involved in DRM over a specified Co plane [11]. The CH_4 decomposition capacity of cobalt nanoparticles was also recognized [12]. Jana et al. showed 33 mol H_2 production per mol of Co from CH_4 at 600 °C. Cobalt–aluminum mixed oxides like Co_2AlO_4 were reduced under a CH_4 stream and can decompose CH_4 further [13]. Using DFT and micro-kinetic modeling, it was found that CH_4 dissociation was a rate-determining step in DRM, and the Cu (111) face also induced surface carbon coupling which tended to form surface carbon clusters and ultimately prompted catalyst deactivation [14]. Gonzalez-Delacruz et al. found that adjacent nickel atoms prevented carbon deposition over cobalt sites, and cobalt sites remained protected from deactivation towards DRM [15]. The Ni and Co bimetallic combination has strong synergy [16]. It nurtures the Ni-Co alloy phase and $NiCo_2O_4$ species over the surfaces of catalysts [17,18]. Ni-Co alloy had excellent CO_2 dissociation ability and weak chemisorption of H_2 and $NiCo_2O_4$ had higher reducibility [17,19]. Ni-Co synergy also increased Ni dispersion over alumina support [20]. Pd could transfer electrons to CO_2 and bring about strong structural changes [21]. Pd–bidentate format species (from a CO_2 carbon source) as well as Pd–CO (from a CH_4 carbon source) [22] justified the strong interaction of Pd with CO_2 as well as CH_4. The spillover of H_2 over Pd was found to increase the reducibility of NiO also [23]. However, the Ni–Pd synergy was found to be greatly dependent on types of support [24]. Ni–Pd-based catalysts are known for a higher coke tolerance compared to monometallic catalysts [25]. Ni–Pd over alumina induced more exposure of Ni° sites with better dispersion of Ni [23].

The idea of dispersion of bimetallic N–Co over an Al_2O_3 support seems more efficient than alumina-supported Ni and alumina-supported Co catalysts. The incorporation of a small amount of Pd along with support may induce CO_2 interaction, NiO reducibility, and CH_4 dissociation over a Ni–Co bimetallic Al_2O_3-supported catalyst. Herein, we have prepared a Pd+Al_2O_3-supported 5wt% Ni–Co catalyst, employed it for DRM, and characterized it with X-ray diffraction, "surface area & porosity", ultra-violet spectroscopy, transmission electron microscopy, temperature-programmed reduction/desorption techniques, and thermogravimetry techniques. The novelty of this research lies in explaining the synergic interaction between different ratios of Ni and Co over a Pd+Al_2O_3 support in terms of surface reducibility, crystallinity, and basicity, which are the regulating factors in DRM activity and coke precipitation. The fine correlation between characterization results and catalytic activity may help to develop a practical DRM catalyst soon.

2. Results

2.1. Characterization Results and Discussion

The X-ray diffraction pattern of fresh and spent xNi(5−x)Co/Pd+Al_2O_3 (x = 5, 3.75, 2.5, 1.25, 0) catalyst systems are shown in Figure 1. The Pd+Al_2O_3-supported 5 wt% Ni catalyst has tetragonal PdO phase (at Bragg's angle 2θ = 34°, 55°, 71.24°; JCPDS reference

number 01-075-0584) and cubic $NiAl_2O_x$ phase (at Bragg's angle 2θ = 37.6°, 39.6°, 45.8°, 61°, 67°; JCPDS reference number 00-020-0776) (Figure 1A). It is interesting to note that after the reaction over the spent-5Ni/Pd+Al_2O_3 catalyst system, the tetragonal PdO phase mostly disappears, and the intensity of the cubic $NiAl_2O_x$ phase is depleted but the cubic alumina phase intensifies. Most of the cubic phase of Al_2O_3 overlaps with the cubic $NiAl_2O_x$ phase excluding the diffraction pattern at 42.8° (JCPDS reference number 00-004-0880). Upon dispersing 3.75 wt% Ni and 1.25 wt% Co active sites together over the Pd+Al_2O_3 support, the same diffraction patterns are observed (Figure 1B). However, the spent 3.75Ni1.25Co/Pd+Al_2O_3 catalyst showed a higher-intensity alumina peak of about 42.8° (than the spent-5Ni/Pd+Al_2O_3) and a new diffraction peak for graphitic carbon (at Bragg's angle 2θ = 26.43°; JCPDS reference number 00-008-0415) [26]. Upon incorporating an equal proportion of Co along with Ni over the Pd+Al_2O_3 support (2.5Ni2.5Co/Pd+Al_2O_3), the intensity of diffraction patterns declines (Figures 1C and S1). Upon a further increase in the proportion of Co in the bimetallic supported system, the 1.25Ni3.75Co/Pd+Al_2O_3 catalyst showed an additional diffraction peak for cubic Co_3O_4 (at Bragg's angle 2θ = 31.22°, 36.81°, 59.2°, 65.11°; JCPDS reference number 01-080-1533) (Figure 1D). The 5Co/Pd+Al_2O_3 catalyst has a lower-intensity peak than the 5Ni/Pd+Al_2O_3 catalyst; the former has cubic $CoAl_2O_4$ mixed oxide phase (at Bragg's angle 2θ = 31.36°, 36.5°, 45.6°, 59.63°, 65.23°; JCPDS reference number 00-003-0896), but the latter has mixed cubic $NiAlO_x$ phase (Figure 1F). The intense diffraction pattern for cubic Al_2O_3 phase (at Bragg's angle 2θ = 37.4°, 42.82°, 45.79°, 67.31°; JCPDS reference number 00-004-0880) is also present over the 5Co/Pd+Al_2O_3 catalyst.

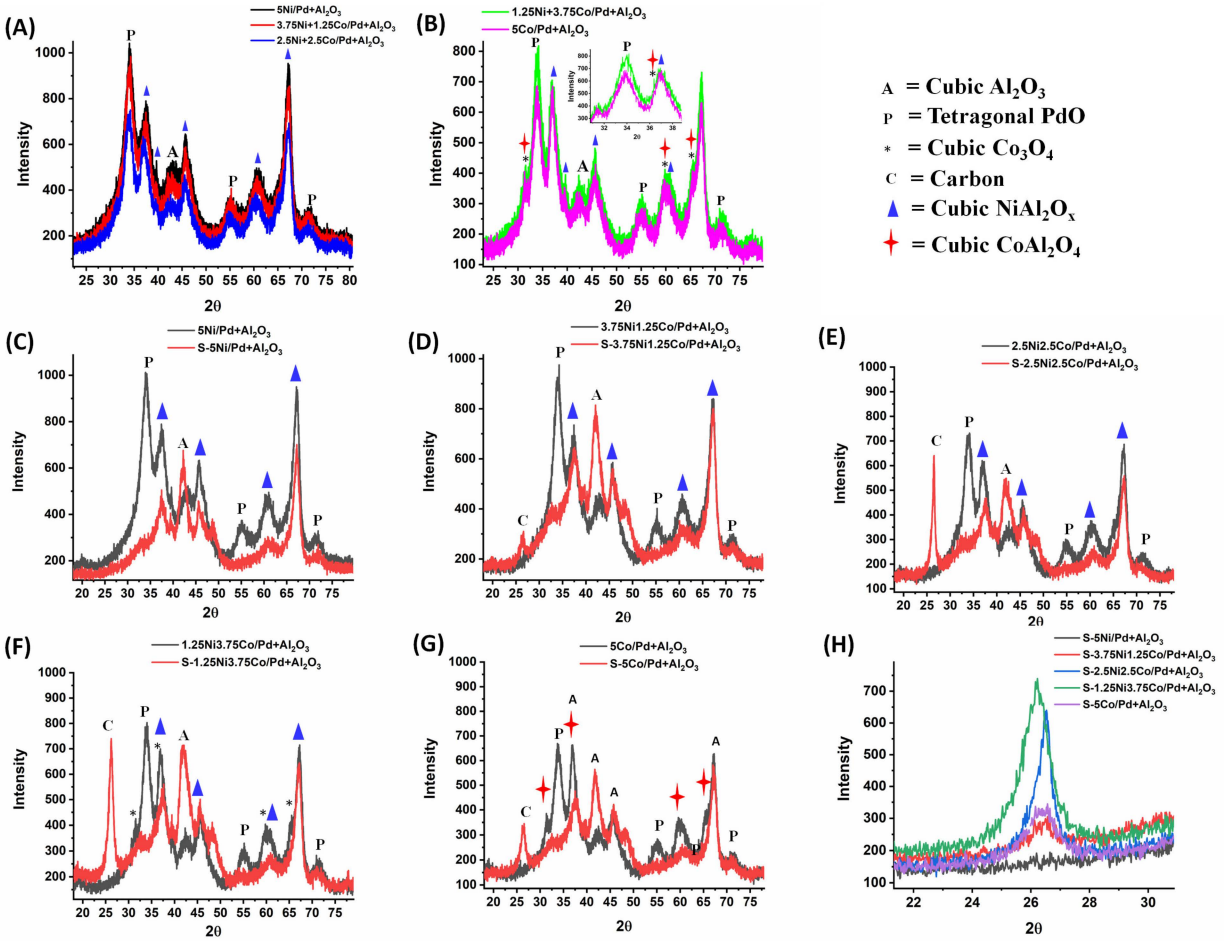

Figure 1. X-ray diffraction pattern of (**A**) xNi(5−x)Co/Pd+Al_2O_3 (x = 5, 3.75, 2.5) catalyst system; (**B**) xNi(5−x)Co/Pd+Al_2O_3 (x = 1.25, 0) catalyst system; (**C**–**G**) fresh and spent xNi(5−x)Co/Pd+Al_2O_3 (x = 5, 3.75, 2.5, 1.25, 0) catalyst system; (**H**) spent xNi(5−x)Co/Pd+Al_2O_3 (x = 5, 3.75, 2.5, 1.25, 0) catalyst system at about 26° Bragg's angle.

The information regarding graphitic carbon peaks over the spent xNi(5−x)Co/Pd+Al_2O_3 (x = 5, 3.75, 2.5, 1.25, 0) catalyst system is needed for emphasis (Figure 1G). Spent 5Ni/Pd+Al_2O_3 has no graphitic carbon peak. Among Ni-Co active sites, upon increasing the Co proportion over Pd+Al_2O_3, the intensity of the crystalline carbon peak increases over the spent catalyst. For spent 1.25Ni3.75Co/Pd+Al_2O_3, the graphitic carbon peak is shifted towards a lower angle, indicating an expansion of lattice parameters in graphitic crystallites. However, the spent 5Co/Pd+Al_2O_3 catalyst shows a diffuse intensity of the graphitic carbon peak. This indicates that graphitic carbon synthesis over the catalyst's surface excels when active sites are composed of two metals.

The N_2 adsorption isotherm and porosity distribution of xNi(5−x)Co/Pd+Al_2O_3 (x = 5, 3.75, 2.5, 1.25, 0) catalysts are shown in Figure 2A,B. The surface area, pore volume, and pore diameter of each catalyst are shown in Figure 2C. All catalysts have a type IV isotherm having an H1 hysteresis loop. This indicates the presence of cylindrical mesopores. The pore size distribution plot (dV/dlogW vs. W) shows a mono-modal pore size distribution of about 8 nm and the average pore size falls between 8.4–8.6 nm. The pore size is not affected much by different loadings of Ni and Co over the Pd/Al_2O_3 support. The pore size distribution and average pore size of catalysts are not affected much upon Ni and Co loading over the Pd/Al_2O_3 support.

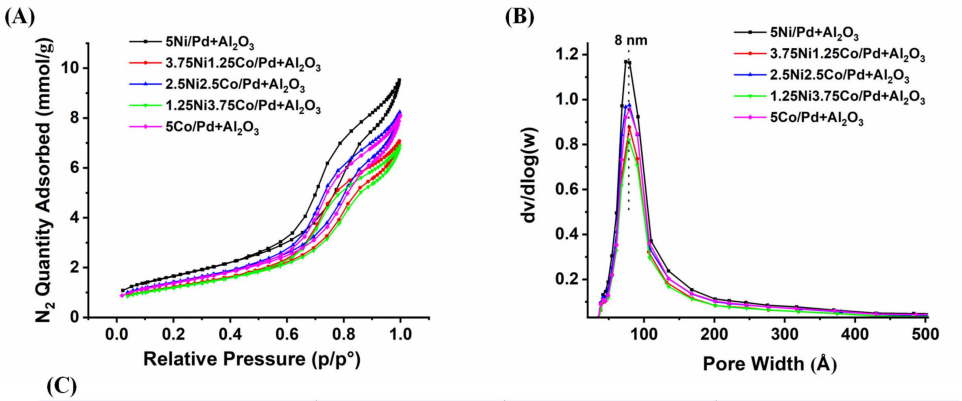

(C)

Catalyst Sample	Surface Area (m^2/g)	Pore Volume (cm^3/g)	Average Pore Size (nm)
5Ni/Pd + Al_2O_3	135.3	0.36	8.4
3.75Ni1.25Co/Pd + Al_2O_3	100.1	0.27	8.5
2.5Ni2.5Co/Pd + Al_2O_3	115.3	0.31	8.4
1.25Ni3.75Co/Pd + Al_2O_3	97.6	0.26	8.4
5Co/Pd + Al_2O_3	112.3	0.30	8.6

Figure 2. (**A**,**B**) The N_2 adsorption isotherm and porosity distribution of xNi(5−x)Co/Pd+Al_2O_3 (x = 5, 3.75, 2.5, 1.25, 0) catalysts. (**C**) Surface area, pore volume, and the average pore size of xNi(5−x)Co/Pd+Al_2O_3 (x = 5, 3.75, 2.5, 1.25, 0) catalysts.

Pd+Al_2O_3-supported Ni has enhanced surface parameters (surface area, pore volume, and pore diameter) compared to the Pd+Al_2O_3-supported Co catalyst. This indicates the extent of interactions of two different metal oxides over the Pd+Al_2O_3 surface. Cobalt oxide crystallites are more readily deposited inside the pores of the Pd+Al_2O_3 support than nickel oxide. 5Ni/Pd+Al_2O_3 has a 135 m^2/g surface area, a 0.37 cm^3/g pore volume, and a 8.4 nm pore diameter. If 5 wt% metal loading over the Pd+Al_2O_3 support is maintained by "3.75 wt% Ni and 1.25 wt% Co", the surface area is decreased by 25% whereas pore volume is diminished by 27% compared to the 5Ni/Pd+Al_2O_3 catalyst. This indicates that the dispersion of bimetallic oxide (Ni and Co) is not as similar as the dispersion of monometallic nickel oxide over the Pd+Al_2O_3 support. Some of the metal oxides may also diffuse into the pores and diminish the surface area and pore volume over the 3.75Ni1.25Co/Pd+Al_2O_3 catalyst more so than the 5Ni/Pd+Al_2O_3 catalyst.

However, if an equal proportion of Ni and Co is dispersed over the $Pd+Al_2O_3$ support, surface area, and pore volume are improved in comparison to the rest of the supported bimetallic systems. This indicates that equal proportions of both Ni and Co have a better interaction with the $Pd+Al_2O_3$ catalyst than the rest of the supported bimetallic system.

H_2 temperature-programmed reduction (H_2-TPR) profiles of $xNi(5-x)Co/Pd+Al_2O_3$ (x = 5, 3.75, 2.5, 1.25, 0) catalysts are shown in Figure 3A. The $5Ni/Pd+Al_2O_3$ catalyst has a single broad reduction peak in the region of 500–825 °C which is attributed to "strongly interacted reducible NiO" or the reduction of $NiAl_2O_x$ species [27]. Also, in XRD, cubic $NiAl_2O_x$ phase is detected. Previously, metallic Ni exsolved from the reduction of $NiAl_2O_x$ (upon reduction) was claimed to be the cause of the generation of stable catalytic active sites for dry reforming of methane [27]. On decreasing the Ni content to 3.75 wt% and incorporating 1.25 wt% Co over the $Pd+Al_2O_3$ support, the reduction peak intensity for "strongly interacted reducible NiO" is decreased and two new peaks in the low-temperature range of about 100 °C and 375 °C are noticed. However, the total uptake of H_2 is marginally decreased. The previous reduction peak (about 100 °C) represents the reduction of highly dispersed PdO species and the second one (375 °C) represents for the reduction of Co_3O_4 [28–30]. Upon equal proportions of Ni and Co in the $2.5Ni2.5Co/Pd+Al_2O_3$ catalyst, lower reduction temperature peaks (about 100 °C and 375 °C) disappear whereas the peak intensity of about 500–825 °C increases. Here, a fine-tuning between Ni and Co is seen. The enhanced peak intensity of about 500–825 °C may be attributed to the enhanced reduction of strongly interacted NiO species or the reduction of a "strongly interacted highly dispersed CoO_x cluster" [28]. In XRD, the crystalline peak intensity for cubic $NiAl_2O_x$ phase is decreased more so for the $2.5Ni2.5Co/Pd+Al_2O_3$ catalyst than for the $3.75Ni1.25Co/Pd+Al_2O_3$ catalyst. So, it can be said that improving the reduction profile in the temperature range of 500–800 °C is a combined contribution of the reduction of "strongly interacted NiO" and the reduction of "highly dispersed CoO_x species". It is noticeable that, upon increasing the Co content (or decreasing the Ni content) up to 2.5 wt%, the total amount of H_2 consumption decreases or the total concentration of reducible species decreases. In $Pd+Al_2O_3$-supported Ni-Co bimetallic catalysts, if the wt% of Co is increased more so than Ni, the total H_2 consumption of the $1.25Ni3.75Co/Pd+Al_2O_3$ catalyst is greater than that of $2.5Ni2.5Co/Pd+Al_2O_3$. However, the reduction profile of the $1.25Ni3.75Co/Pd+Al_2O_3$ catalyst is altered. The reduction peak for strongly interacted NiO species was suppressed extensively as well as the reduction peaks for PdO species and Co_3O_4 is intensified over the $1.25Ni3.75Co/Pd+Al_2O_3$ catalyst. This indicates that the fine-tuning between Co and Ni is disturbed completely over the $1.25Ni3.75Co/Pd+Al_2O_3$ catalyst. However, it can be said that the presence of a higher wt% of Co may induce a higher population of PdO species to reduce and vice versa. It is noticeable that, over the $5Co/Pd+Al_2O_3$ catalyst, both reduction peak of PdO and Co_3O_4 is shifted to a relatively higher temperature, indicating higher levels of metal–support interaction. Except for when Ni/Co = 1, higher concentrations of reducible Co_3O_4 and PdO species are observed with a decreasing ratio of Ni/Co.

CO_2 temperature-programmed desorption (CO_2-TPD) profiles of $xNi(5-x)Co/Pd+Al_2O_3$ (x = 5, 3.75, 2.5, 1.25, 0) catalysts are shown in Figure 3B. It is categorized into three basic regions. The CO_2 desorption peak is about 100 °C for weak basic sites, about 300 °C for moderate-strength basic sites, and about 700 °C for strong basic sites [31]. The basicity of the surface is contributed to by surface hydroxyl and surface oxygen [32]. Surface hydroxyl constitutes weak basicity. The surface oxygen which generates carbonate/formate intermediate upon interaction with CO_2 is related to medium-strength basic sites. The surface oxygen which generates more stable carbonates upon reaction with CO_2 constitutes strong basic sites [31,33]. From the CO_2-TPD, a general observation can be pointed out. The total amount of CO_2-desorbed gases is decreased with increasing Co amounts up to 2.5 wt% (or decreasing Ni amounts to 2.5 wt%). Upon further increasing the Co loading, the CO_2-desorbed amount is increased over the $1.25Ni3.75Co/Pd+Al_2O_3$ catalyst. The CO_2-TPD profile representing a higher loading of Co than Ni over the $5Co/Pd+Al_2O_3$

support has a different look than the rest of the catalyst. It has an additional peak of about 850 °C. The peak intensity of about 850 °C is increased upon further loading of Co. This indicates that the CO_2 desorption peak is related to the interaction of CO_2 over Co. It can also be said that CO_2 strongly interacts with Co, more so than Ni.

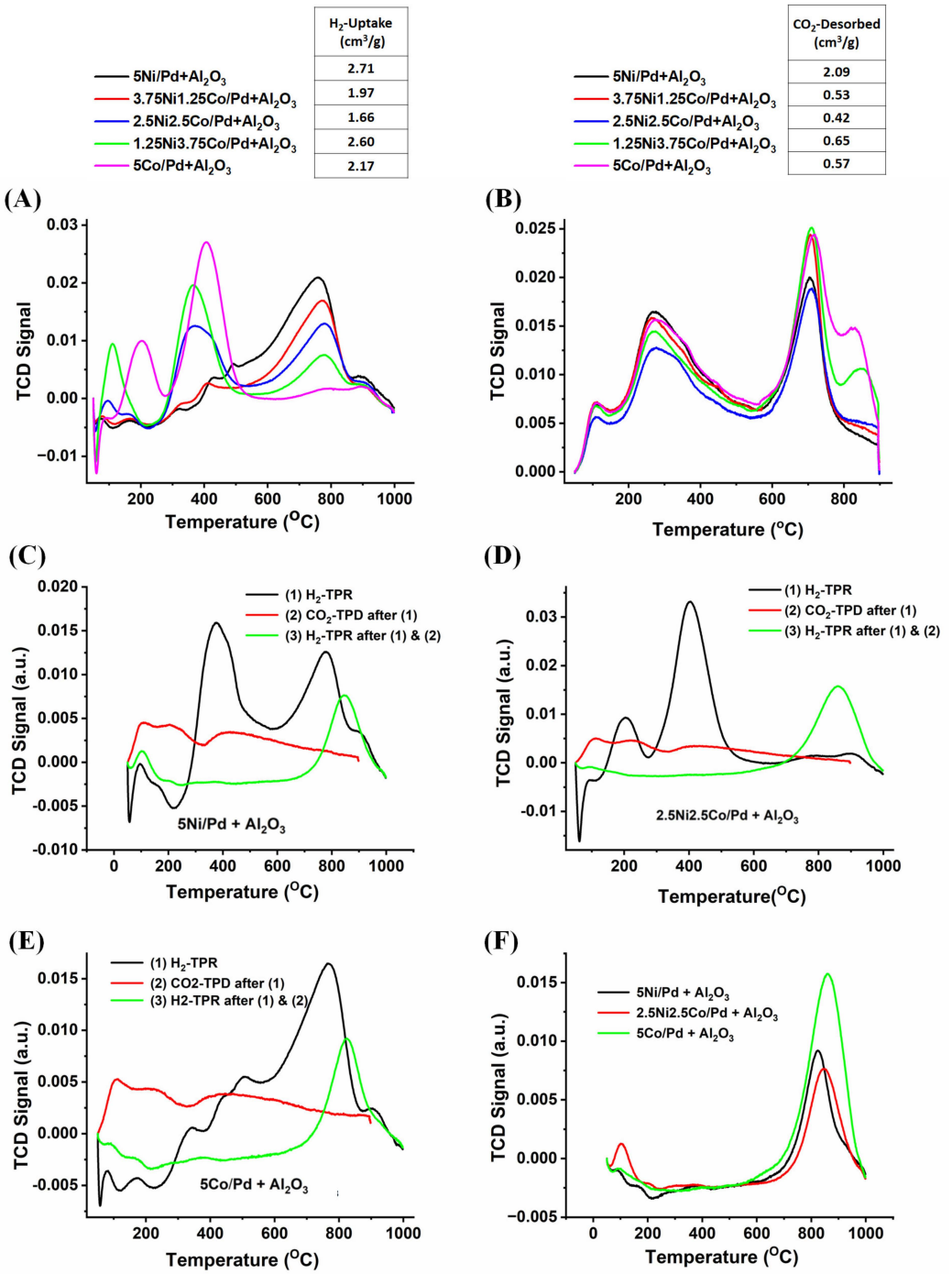

Figure 3. (**A**) H_2-TPR of xNi(5−x)Co/Pd+Al_2O_3 (x = 5, 3.75, 2.5, 1.25, 0) catalysts and the inset table shows total H_2 uptake by each catalyst; (**B**) CO_2-TPD of reduced-xNi(5−x)Co/Pd+Al_2O_3 (x = 5, 3.75, 2.5, 1.25, 0) catalysts and the inset table shows total amount of CO_2 desorbed over each catalyst; (**C**) cyclic H_2TPR–CO_2TPD–H_2TPR of 5Ni/Pd+Al_2O_3; (**D**) cyclic H_2TPR-CO_2TPD-H_2TPR of 2.5Ni2.5Co/Pd+Al_2O_3; (**E**) cyclic H_2TPR–CO_2TPD–H_2TPR of 5Co/Pd+Al_2O_3; (**F**) last reductive treatment in cyclic H_2TPR–CO_2TPD–H_2TPR experiments of xNi(5−x)Co/Pd+Al_2O_3 (x = 5, 2.5, 0) catalysts.

The cyclic H_2TPR–CO_2TPD–H_2TPR experiments for xNi(5−x)Co/Pd+Al_2O_3 (x = 5, 2.5, 0) catalysts are shown in Figure 3C–E. After sequential H_2-TPR (reduction), CO_2-TPD (oxidation), and H_2-TPR (reduction) treatments of the catalyst, a reducible peak of about 750–900 °C is observed. The reduction peak in such a high-temperature range was previously attributed to the reduction of NiO which was supported over M–O–M′ (M ≠ M′; M = W, Zr, Al and M′ = W, Zr, Al) species [34,35]. Here also, the reduction of NiO or Co_3O_4 over a Pd–O–Al support can be expected at such a high reduction temperature. The cyclic H_2TPR–CO_2TPD–H_2TPR experiments indicate that under high-temperature reactions (800 °C), some of the active species, such as Ni and Co, are regenerated into NiO and Co_3O_4 under the CO_2 stream (which is reduced by the last reductive treatment). This indicates that under the oxidizing environment (in the CO_2 stream) during DRM, some active sites are oxidized and become inactive for further catalyzing DRM reactions. It can be noticed that the intensity of such a peak is maximal for the 5Co/Pd+Al_2O_3 catalyst (Figure 3F).

The bandgap of xNi(5−x)Co/Pd+Al_2O_3 (x = 5, 3.75, 2.5, 1.25, 0) catalysts and thermogravimetry analysis of spent xNi(5−x)Co/Pd+Al_2O_3 (x = 5, 3.75, 2.5, 1.25, 0) catalysts are shown in Figure 4. Without Co, the bandgap is 1.58 eV over 5Ni/Pd+Al_2O_3. It is noticeable that the band gap between the valence band and conduction band is continuously decreasing as the proportion of Co is increased in xNi(5−x)Co/Pd+Al_2O_3 (x = 0,1.25, 2.5, 3.75, and 5) catalysts. The band gap is minimal (0.34 eV) over the 5Co/Pd+Al_2O_3 catalyst. Thermogravimetric analyses of fresh and spent xNi(5−x)Co/Pd+Al_2O_3 (x = 5, 3.75, 2.5, 1.25, 0) catalysts are carried out and shown in Figure 4B. The fresh catalyst samples have minimal loss compared to the spent catalyst samples. The TGA results indicate that Pd+Al_2O_3-supported Ni catalysts have minimal coke decomposition (~4% weight loss) whereas, upon introduction of just 1.25 wt% Co (along with 3.75 wt% Ni) over the Pd+Al_2O_3 support, the coke deposition is exceptionally high (46.87%). Upon increasing the proportion of Co further, the coke deposition is decreased. The 2.5Ni2.5Co/Pd+Al_2O_3 catalyst shows ~21% weight loss whereas ~11–13% weight loss is evident over 1.25Ni3.75Co/Pd+Al_2O_3 and 5Co/Pd+Al_2O_3 catalysts. To confirm the carbon type, Raman analysis of spent catalyst samples is undertaken (Figure 4C). All catalysts have three Raman bands at 1070 cm^{-1}, 1340 cm^{-1}, and 1570 cm^{-1} for vibration of C–C sp^3 (T band), defect carbon (D band), and ordered carbon (G band), respectively [36], [37] Interestingly, D bands and G bands are most intense for the spent 3.75Ni1.25Co/Pd+Al_2O_3 catalyst. Thus, it can now be concluded that over the spent 3.75Ni1.25Co/Pd+Al_2O_3 catalyst had a maximal coke deposit and the coke deposit was mostly sp^2 hybridized carbon with defective and ordered carbon structures. The relatively higher intense C–C sp^3 (T band) is noticed over the spent 5Co/Pd+Al_2O_3 catalyst (more so than other catalysts).

Transmission electron microscopy of catalysts and particle size distribution are depicted in Figure 5. In spent catalyst samples, the larger particle size is clearly evident. In the case of the spent 5Ni/Pd+Al_2O_3 catalyst, no carbon formation is noticed but over the spent 2.5Ni2.5Co/Pd+Al_2O_3 catalyst, carbon nanotubes are visualized easily. In the XRD, the diffraction pattern for graphitic carbon was absent. This indicates that 5Ni/Pd+Al_2O_3 is coke-resistant.

2.2. Catalytic Activity Results and Discussion

Catalytic activity results of xNi(5−x)Co/Pd+Al_2O_3 (x = 5, 3.75, 2.5, 1.25, 0) catalysts in terms of H_2 yield (%) and CO yield (%) are shown in Figure 6A,B. The activity experiments were reproduced twice for all the catalysts. It was noted that the error of catalytic activity was 2–4% for all the experiments. The catalytic activity results and TOF results (at the end of 430 min TOS) are also shown in tabular form in Figure 6C. H_2 yield vs. the H_2/CO ratio of catalysts is presented in Figure S1. After the decomposition of CH_4 over active sites (into CH_{4-x}; x = 1–4) over different catalyst systems, two phenomena ran parallel. One is the oxidation of CH_{4-x} by CO_2, leading to DRM reaction, and another is the polymerization of CH_{4-x} species, leading to coke deposit. Further, the coverage of inert carbon species

over active sites may seriously affect DRM activity. Apart from the coke deposit, if only DRM reactions take place over a catalyst, the H_2 yield and CO yields should be similar ($CO_2 + CH_4 \rightarrow 2CO + 2H_2$). But here, the CO yield is always found to be above the H_2 yield over each catalyst system. This indicates the presence of a reverse water gas shift reaction which consumes the H_2 ($CO_2 + H_2 \rightarrow CO + H_2O$) and so the CO yield surpasses the H_2 yield.

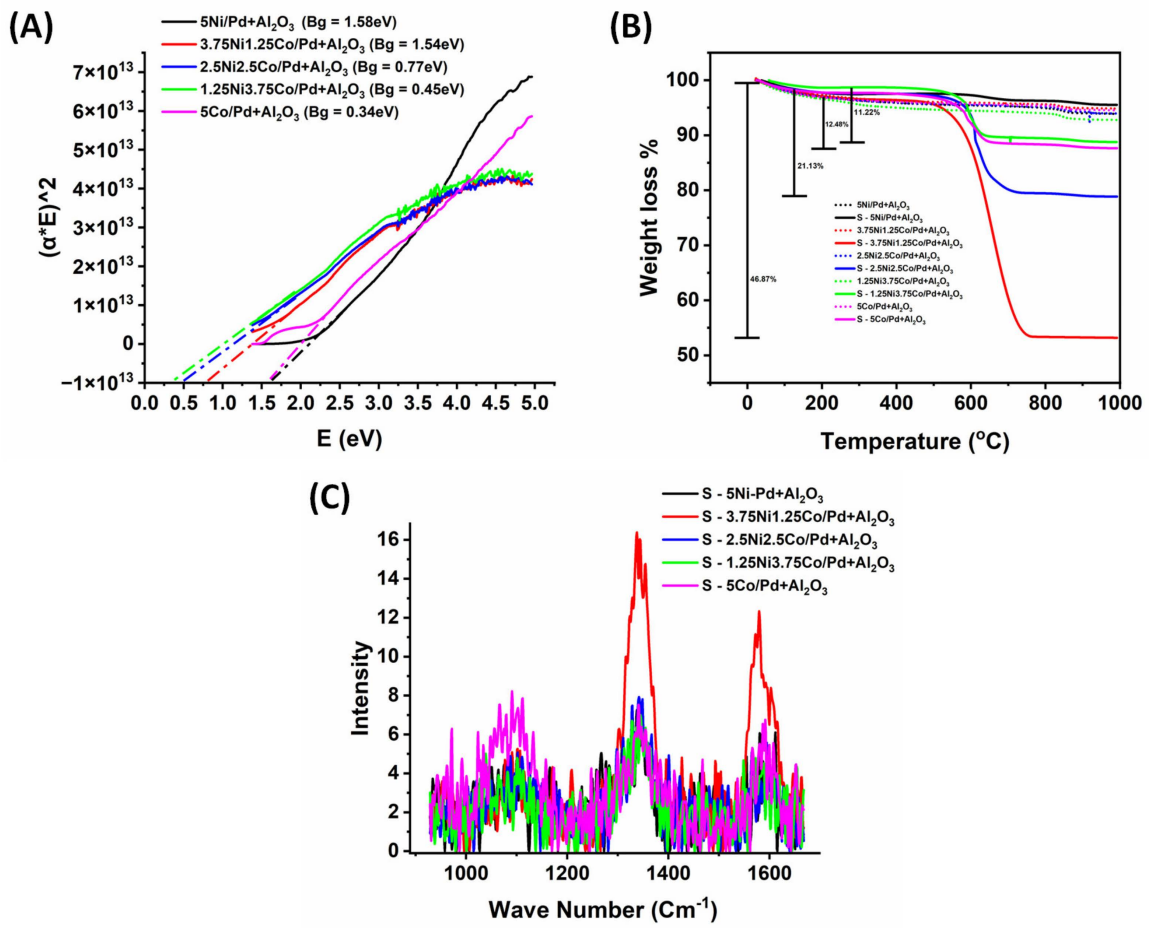

Figure 4. (**A**) The bandgap of xNi(5−x)Co/Pd+Al_2O_3 (x = 5, 3.75, 2.5, 1.25, 0) catalysts. (**B**) Thermogravimetry analysis of fresh and spent xNi(5−x) Co/Pd+Al_2O_3 (x = 5, 3.75, 2.5, 1.25, 0) catalysts. The dotted thermogravimetry curves are shown for fresh catalyst samples. (**C**) Raman spectra of spent xNi(5−x) Co/Pd+Al_2O_3 (x = 5, 3.75, 2.5, 1.25, 0) catalysts.

The H_2-TPR and CO_2-TPD profiles of the catalyst systems reflect the information regarding the catalysts' reducibility and basicity (extent of CO_2 interaction). A general trend of reducibility and basicity over xNi(5−x)Co/Pd+Al_2O_3 (x = 5, 3.75, 2.5, 1.25, 0) catalysts is observed. Upon decreasing the Ni wt% from 5 to 2.5 (or increasing the Co wt% from 0–2.5), the total H_2 consumption and CO_2 desorption of the catalyst are decreased from 2.7 to 1.7 cm^3/g and from 2.1 to 0.4 cm^3/g, respectively. This means that total reducibility and total basicity (CO_2 interaction) are decreased upon increasing the Co proportion up to 2.5 wt% over xNi(5−x)Co/Pd+Al_2O_3 (x = 5, 3.75, 2.5, 1.25, 0) catalyst systems. However, the catalyst activity results of xNi(5−x)Co/Pd+Al_2O_3 (x = 5, 3.75, 2.5, 1.25, 0) catalysts do not follow this trend. The 3.75Ni1.25Co/Pd+Al_2O_3 catalyst has minimal catalytic activity among bimetallic catalysts. This indicates that only total reducibility and total basicity do not monitor the reaction. Other factors like types of reducible species, types of surface basic species, total carbon deposits, and types of carbon in deposit should also be considered.

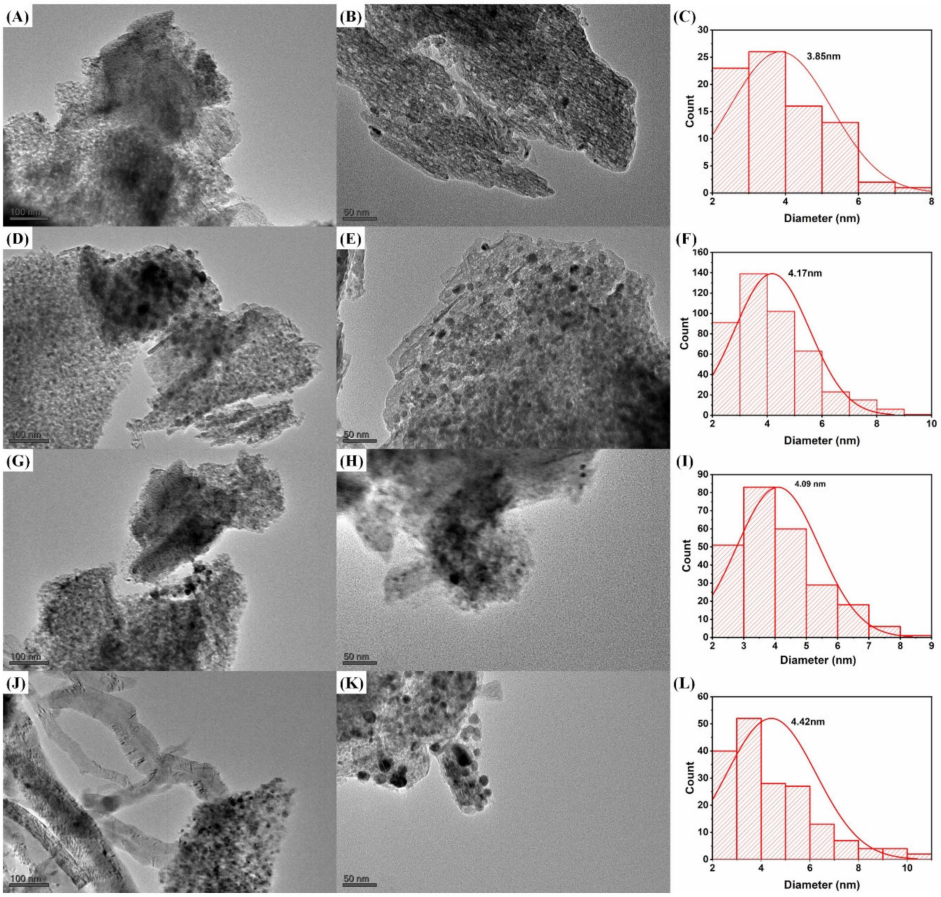

Figure 5. TEM image of (**A**) 5Ni/Pd+Al_2O_3 on 100 nm scale; (**B**) TEM image of 5Ni/Pd+Al_2O_3 on 50 nm scale; (**D**) spent 5Ni/Pd+Al_2O_3 on 100 nm scale; (**E**) spent 5Ni/Pd+Al_2O_3 on 50 nm scale; (**G**) 2.5Ni2.5Co/Pd+Al_2O_3 on 100 nm scale; (**H**) 2.5Ni2.5Co/Pd+Al_2O_3 on 50 nm scale; (**J**) spent 2.5Ni2.5Co/Pd+Al_2O_3 on 100 nm scale; (**K**) spent 2.5Ni2.5Co/Pd+Al_2O_3 on 50 nm scale; Particle size distribution of (**C**) 5Ni/Pd+Al_2O_3; (**F**) spent 5Ni/Pd+Al_2O_3; (**I**) 2.5Ni2.5Co/Pd+Al_2O_3; (**L**) spent 2.5Ni2.5Co/Pd+Al_2O_3.

Ni supported over Pd+Al_2O_3 has a stable Ni site derived from the reduction of cubic $NiAl_2O_x$ phases. The TGA result of the spent 5Ni/Pd+Al_2O_3 catalyst shows the presence of a minimum carbon deposit (4% weight loss) and the Raman result shows the presence of both diamond and graphitic carbon bands over the spent 5Ni/Pd+Al_2O_3 catalyst. Regarding the carbon deposit, due to the lesser amount of graphitic carbon over the spent 5Ni/Pd+Al_2O_3 catalyst, a graphic carbon crystalline peak is not observed in XRD analysis. The 5Ni/Pd+Al_2O_3 catalyst does not show crystalline carbon peaks after the DRM reaction. It seems that the catalytic active Ni site derived from $NiAl_2O_x$ is highly stable; it dissociates the CH_4 (into CH_{4-x}; x = 1–4) and it also resists the accumulation of CH_{4-x} species for oligomerization. Cobalt supported over Pd+Al_2O_3 also has active Co sites derived from the cubic Co_3O_4 phase. The stability of the 5Ni/Pd+Al_2O_3 catalyst's active sites is higher than those derived from the 5Co/Pd+Al_2O_3 catalyst. The instability of Co active sites is also evident in the cyclic H_2TPR–CO_2TPD–H_2TPR experiment. The cyclic experiment shows the highest-intensity reduction peak at about 800 °C (in the last reductive treatment) over 5Co/Pd+Al_2O_3, indicating the oxidation of active Co species (or inactiveness of active sites) by CO_2 during DRM. Further, the spent 5Co/Pd+Al_2O_3 catalyst also has a remarkable peak intensity of graphitic carbon whereas, over the spent 5Ni/Pd+Al_2O_3 catalyst, the graphitic carbon peak is absent. TGA results are similar. The spent 5Ni/Pd+Al_2O_3 catalyst has minimal weight loss (4.13%) whereas the spent 5Co/Pd+Al_2O_3 catalyst has three times more weight loss. The spent 5Ni/Pd+Al_2O_3

catalyst has no graphitic carbon but a small amount of oxidizable carbon deposit whereas the spent 5Co/Pd+Al_2O_3 catalyst has marked growth of both amorphous and graphitic carbon deposits. Altogether, the 5Ni/Pd+Al_2O_3 catalyst has higher and constant activity and a 57–56% H_2 yield after 430 min on stream. The catalyst activity of 5Co/Pd+Al_2O_3 is lowest (43% H_2 yield) and it declines very fast (34% H_2 yield) within the 430-minute timeframe on stream. The H_2/CO ratio of the 5Ni/Pd+Al_2O_3 catalyst is a maximum (0.87) whereas it is a minimum (0.78) over 5Co/Pd+Al_2O_3 (Figure S1). Low H_2 production over 5Co/Pd+Al_2O_3 results in a lower H_2/CO ratio of the catalyst. The major cause of inferior activity over 5Co/Pd+Al_2O_3 seems to be due to less stable active sites vis-à-vis relatively higher coke deposition during DRM reactions.

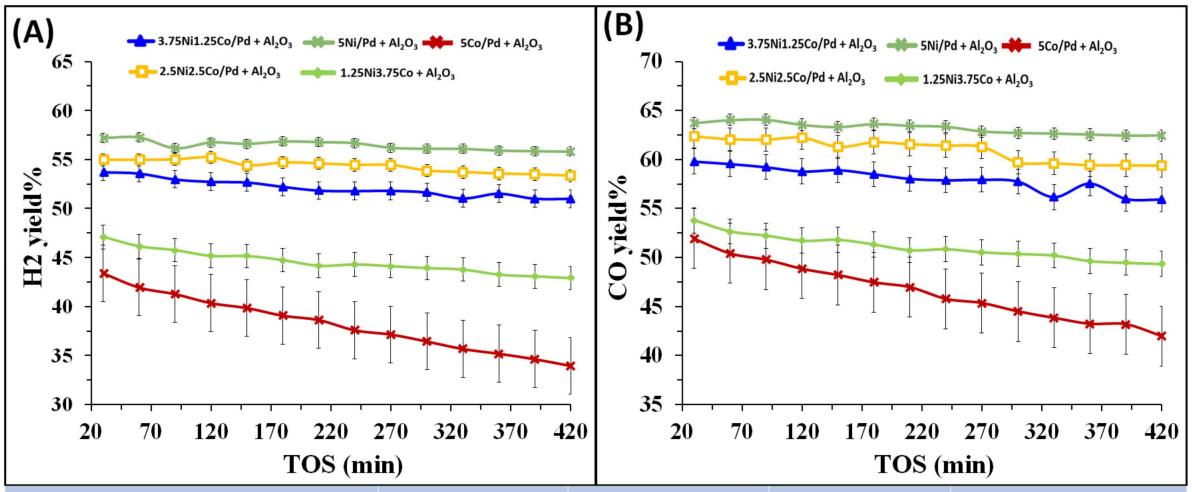

(C)

Catalyst	H_2 Yield (%)	CO Yield (%)	Weight loss (%)	TOF (h^{-1})
5Ni/Pd + Al_2O_3	55.81	62.44	4.53	149.72
3.75Ni1.25CO/Pd + Al_2O_3	50.99	55.90	11.22	99.85
2.5Ni2.5CO/Pd + Al_2O_3	53.34	59.38	12.48	165.01
1.25Ni3.75CO/Pd + Al_2O_3	42.91	49.35	21.13	108.64
5CO/Pd + Al_2O_3	33.95	41.97	46.87	58.23

Figure 6. Catalytic activity results of xNi(5−x)Co/Pd+Al_2O_3 (x = 5, 3.75, 2.5, 1.25, 0) catalysts: (**A**) H_2-yield (%) vs. time on stream (TOS) with error bar; (**B**) CO yield (%) vs. time on stream with error bar; (**C**) H_2 yield (%), CO yield (%), and weight loss (%) (from TGA results) after 430 min on stream.

Upon incorporation of 1.25 wt% Co along with 3.75 wt% Ni over a Pd+Al_2O_3 support, the catalyst experiences in a sharp drop in surface area and pore volume. The surface of 3.75Ni1.25Co/Pd+Al_2O_3 is populated by relatively lesser amounts of catalytic active Ni species (derived from $NiAl_2O_4$) or catalytic active Co (derived from dispersed CoO_x species) and Co species derived from Co_3O_4 species. The XRD patterns show a higher intensity of graphitic carbon (than 5Ni/Pd+Al_2O_3) and the TGA result shows extensive weight loss over the spent 3.75Ni1.25Co/Pd+Al_2O_3 catalyst. This indicates, upon incorporating Co, that the distribution of reducible surface species is modified greatly and brings DRM and carbon deposition. The most intense Raman band over the spent 3.75Ni1.25Co/Pd+Al_2O_3 catalyst again confirms the high-level coke deposit over the catalyst. Raman analysis of catalysts showed that these carbon deposits belong to sp^2 hybridized defective diamond carbon (D band) and ordered graphitic carbon (G) structures. In total, the catalytic activity of 3.75Ni1.25Co/Pd+Al_2O_3 is decreased (54–51% H_2 yield during 430 min of TOS) but weight loss is increased extensively (~47%) with respect to the 5Ni/Pd+Al_2O_3 catalyst.

Dispersing an equal proportion of Ni and Co over the Pd+Al_2O_3 catalyst shows a decrease in total crystallinity and an adequate population of catalytic active Co or Ni species, which is derived by the reduction of CoO_x or $NiAl_2O_x$ species (strongly interacted reducible species). Interestingly, frequently observed reducible species like PdO and Co_3O_4 are completely absent over the 2.5Ni2.5Co/Pd+Al_2O_3 catalyst. The surface area and pore volume of the 2.5Ni2.5Co/Pd+Al_2O_3 catalyst also progress more than those of the 3.75Ni1.5Co/Pd+Al_2O_3 catalyst. The TOF of 2.5Ni2.5Co/Pd+Al_2O_3 catalyst is found to be 165 h^{-1} which is greater than that of other catalyst systems in this study (Figure 6C). The H_2/CO ratio of the 2.5Ni2.5Co/Pd+Al_2O_3 catalyst, again, reaches the maximum, 0.87 (equal to the 5Ni/Pd+Al_2O_3 catalyst). The total carbon deposit over the spent 2.5Ni2.5Co/Pd+Al_2O_3 catalyst decreases impressively but graphitic carbon is still intensified along with Co loading. Despite the strong tuning of Co and Ni in favor of DRM reactions, the catalytic activity is improved with respect to the 3.75Ni1.5Co/Pd+Al_2O_3 catalyst but is not better than that if the 5Ni/Pd+Al_2O_3 catalyst. Overall, the evolution of stable active sites over the more expanded 2.5Ni2.5Co/Pd+Al_2O_3 catalyst surface results in an enhancement in catalytic activity (55–53% H_2 yield after 430 min) with respect to the 3.75Ni1.5Co/Pd+Al_2O_3 catalyst.

The incorporation of a greater amount of Co than Ni over Pd+Al_2O_3 causes a depletion in the reduction peak at high temperatures as well as a rise in the reduction peak at low and intermediate temperatures. This indicates the loss of strongly interacted active sites (derived from the reduction of $NiAl_2O_x$ and dispersed CoO_x species) from the catalyst surface. However, cobalt-related stable carbonates are observed over the 1.25Ni3.75Co/Pd+Al_2O_3 catalyst. XRD spectra of the spent catalyst also showed the highest intensity peak for graphitic carbon. Overall, it can be said that the lack of strongly interacted active sites and potential graphitic carbon deposits over the 1.25Ni3.75Co/Pd+Al_2O_3 catalyst resulted in the lowest catalyst performance among bimetallic supported catalysts. The 1.25Ni3.75Co/Pd+Al_2O_3 catalyst showed a 43% H_2 yield with a markable decrease in H_2/CO (0.84) after 430 min on stream.

Overall, the 2.5Ni2.5Co/Pd+Al_2O_3 catalyst showed the highest TOF and activity among the bimetallic catalysts investigated in this study. A comparative table of the different catalyst systems is shown in Table 1. By comparing the catalytic activity results with closely related catalysts, the current catalyst system was found to be more effective than others.

Table 1. The comparative table of catalytic activity (in terms of H_2-yield) over different catalyst systems.

Sr. No.	Catalyst Name	Active Sites (wt.%)	CP	AC (g)	GHSV (L/h g_{cat})	RT (°C)	TOS (h)	Y (H_2) %	Ref.
1	Ni/ZrO_2-I	10 (Ni)	I	0.05	60	700	-	50	[38]
2	Ni/ZrO_2	5 (Ni)	I	0.1	42	700	7	43	[39]
3	Ni/CeO_2-$ZrO_2$75	5 (Ni)	Co-I	0.1	30	700	24	28	[40]
4	Ni1Ce/ZrO_2	5 (Ni)	I	0.1	42	700	7	47	[41]
5	Ni/18wt%CeO_2-82wt%ZrO_2	8 (Ni)	I	0.15	40	750	50	35	[40]
6	Ni/28mol%CeO_2-72mol%ZrO_2	5 (Ni)	I	0.1	30	700	21	35	[40]
7	Ni/SiO_2	5 (Ni)	I	0.1	24	700	23	22	[23]
8	Ni-SiO_2-OA	5 (Ni)	I-OA	0.1	24	700	23	25	[23]
9	Ni-MSN	5 (Ni)	I	0.1	36	700	25	49	[42]
10	Ni/Al_2O_3	10 (Ni)	I	-	70	600	70	22.7	[38]

Table 1. *Cont.*

Sr. No.	Catalyst Name	Active Sites (wt.%)	CP	AC (g)	GHSV (L/h g_{cat})	RT (°C)	TOS (h)	Y (H_2) %	Ref.
11	Ni3TiAl	5 (Ni)	MM	0.1	42	700	7	30	[27]
12	Ni3MoAl	5 (Ni)	MM	0.1	42	700	7	39	[27]
13	Ni/CeO_2-Al_2O_3	10 (Ni)	M1	0.1	30	750	12	12.5	[43]
14	5Ni/5Y-Zr	5 (Ni)	Sg	0.1	42	700	7	45	[44]
15	5Ni/5Mg-Zr	5 (Ni)	Sg	0.1	42	700	7	23	[44]
16	2.5Ni2.5Co/Pd+Al_2O_3	5 (Ni & Co)	I	0.1	42	800	7	53	This Study

CP: Catalyst's Preparation Method, AC: Amount of catalyst taken for the reaction, RT: Reaction temperature, TOS: Time on stream, Y: Yield, MSN: Mesoporous Silica Nanoparticle, I: Impregnation method, Co-I: Coprecipitation followed by impregnation, Sg: Sol-gel method, MM: Mechanical mixing, Method 1 (M1): The support is prepared by 0.5–1.2 nm diameter Al_2O_3 sphere saturated by 5 wt.% ceria solution.

3. Materials and Methods

3.1. Catalyst Preparation

The xNi(5−x) Co/Pd+Al_2O_3 (x = 5, 3.75, 2.5, 1.25, 0) catalysts were prepared using a wet impregnation method using nitrate precursor solutions of Co and Ni and a 5 wt% Pd+Al_2O_3 (Aldrich Chemical Co., Milwaukee, WI, USA) support. Nickel nitrate hexahydrate ($Ni(NO_3)_26H_2O$; 99% purity, Fisher, Schwerte, Germany) and cobalt nitrate hexahydrate ($Co(NO_3)_26H_2O$; 99% purity, Aldrich Chemical Company Inc., Milwaukee, WI, USA) were dissolved in distilled water and stirred continuously to form a uniform solution. Thereafter, the catalyst support (5 wt% Pd+Al_2O_3) was added to the precursor solution. The mixture was stirred under heating until a paste was formed. Further, the paste was dried for 12 h at 120 °C and calcined at 600 °C calcination for 3 h. All elements claimed in the catalyst synthesis were confirmed by EDX analysis (Figure S2). The catalysts were abbreviated as xNi(5−x)Co/Pd+Al_2O_3 (x = 5, 3.75, 2.5, 1.25, 0) where x is wt%.

3.2. Catalyst Performance Evaluation

The dry reforming of methane reaction was carried out over 0.1 g catalysts at 800 °C at 1 atm pressure in a packed-bed stainless steel reactor (internal diameter of 0.91 mm and a length of 30 cm, PID Eng. and Tech Micro Activity) equipped with a K-type stainless steel sheathed thermocouple. An axially positioned thermocouple close to the catalyst bed was used to monitor the reaction temperature. Before the reaction, the catalyst was reduced/activated under H_2 at 800 °C for 60 min then again after the remnant H_2 was purged by N_2. After catalyst activation, a DRM gas feed (CH_4:CO_2:N_2 in the volume ratio of 3:3:1, respectively) was passed through the catalyst bed with 42,000 mL/($g_{cat.}$h) space velocity at an 800 °C reaction temperature for 430 min on stream. The gas composition in the outlet stream was analyzed online using a gas chromatograph (Shimadzu GC-2014, Kyoto, Japan) equipped with a thermal conductivity detector. H_2 yield percent, CO yield percent, and TOF (h^{-1}) were calculated from the following formula [45]:

$$H_2 \text{ yield } (\%) = \frac{\text{Mole of } H_2 \text{ in Product}}{2 \times \text{Mol of } CH_{4in}} \times 100 \quad (1)$$

$$\text{CO yield } (\%) = \frac{\text{Mole of CO in Product}}{\text{Mol of } CH_{4in} + \text{Mol of } CO_{2in}} \times 100 \quad (2)$$

$$\text{TOF } (h^{-1}) = \frac{v_{CH_4} \times X_{CH_4} \times P}{R \times T \times S_{Ni+Co}} \quad (3)$$

v_{CH_4} = Flow rate of methane, X_{CH_4} = Conversion ratio of methane, P = Pressure in atm, R = Gas constant in $L{\cdot}atm{\cdot}K^{-1}{\cdot}mol^{-1}$, T $\frac{1}{4}$= Temperature in Kelvin, S_{Ni+Co} = The mole of surface Ni and Co atoms in the sample.

3.3. Catalyst Characterization

The catalysts were characterized by X-ray diffraction, surface area and porosity, ultraviolet spectroscopy, H_2 temperature-programmed reduction (H_2-TPR), CO_2 temperature-programmed desorption (CO_2-TPD), cyclic H_2TPR–CO_2TPD–H_2TPR experiments, thermogravimetry analysis, and transmission electron microscopy. Detailed instrument specifications and analysis procedures are described in the supporting information file.

4. Conclusions

To conclude, 5 wt% Ni over a Pd+Al_2O_3 catalyst has Ni as active sites that are derived primarily from strong metal–support interaction species (or $NiAl_2O_x$) and it is oxidized the least under a CO_2 stream at a DRM reaction temperature. It has no graphitic carbon deposit and acquires the highest 57–56% H_2 yield. Further, 5 wt% Co over the Pd+Al_2O_3 catalyst has Co as active sites that are derived from Co_3O_4 and the active sites are oxidized exclusively under a CO_2 stream during DRM reactions. The 5Co/Pd+Al_2O_3 catalyst has the least activity (43–34% H_2-yield) and a markable graphitic carbon deposit. Upon introducing a 1.25 wt% cobalt proportion in the Ni-Co bimetallic catalyst over a Pd+Al_2O_3 support, the graphitic carbon deposit is enhanced abruptly. Total reducibility and the extent of CO_2 interaction are decreased upon increasing the Co proportion up to 2.5 wt% over xNi(5−x)Co/Pd+Al_2O_3 (x = 5, 3.75, 2.5, 1.25, 0) catalyst systems. Incorporation of 1.25 wt% Co along with 3.75 wt% Ni over Pd+Al_2O_3 results in fewer active sites derived from strong metal–support interaction species ($NiAl_2O_x$ or dispersed CoO_x species), resulting in extensive oxidizable carbon deposits, higher-level graphitic carbon deposits, and relatively less DRM activity (54–51% H_2 yield) compared to 5Ni/Pd+Al_2O_3. Upon incorporation of an equal amount of Co and Ni over Pd+Al_2O_3, the catalyst's crystallinity decreases and, again, nurtures a higher number of active sites derived from strong metal–support interaction species. The TOF of the 2.5Ni2.5Co/Pd+Al_2O_3 catalyst is a maximum 165 h^{-1} and the H_2/CO ratio of the 2.5Ni2.5Co/Pd+Al_2O_3 catalyst, again, reaches the maximum 0.87 (equal to 5Ni/Pd+Al_2O_3 catalyst). Among all bimetallic supported catalysts, the catalyst performance of the 1.25Ni3.75Co/Pd+Al_2O_3 catalyst is inferior due to the deficit of strong metal–support interaction species and the highest level of graphitic carbon deposits.

Supplementary Materials: The following supporting information can be downloaded at: https://www.mdpi.com/article/10.3390/catal13101374/s1, Supporting information S1: Details specification and procedure of characterization technique, Figure S1: H_2-yield and H_2/CO ratio over different catalyst systems; 5Ni~5Ni//Pd+Al_2O_3, 3.75Ni1.25Co~3.75Ni1.25Co/Pd+Al_2O_3, 2.5Ni2.5Co~2.5Ni2.5Co/Pd+Al_2O_3, 1.25Ni3.75Co~1.25Ni3.75Co/Pd+Al_2O_3, 5Co~5Co/Pd+Al_2O_3. Figure S2: EDX profile of (A) 5Ni/Pd+Al_2O_3 (B) 2.5Ni2.5CO/Pd+Al_2O_3 (C) 1.25Ni3.75CO/Pd+Al_2O_3.

Author Contributions: Methodology, A.H.F., A.E.A. and A.S.A.-F.; Conceptualization, A.H.F., A.S.A.-F. and D.M.V.; Writing—original draft preparation, D.M.V. and A.H.F.; Editing, A.A.I., R.K. and A.S.A.-F.; Data curation: N.A., A.A.I. and D.M.V.; Software, M.F.A., N.A. and D.M.V.; Investigation, A.H.F., A.A.I. and A.S.A.-F., Formal Analysis: A.E.A. and N.A.; Visualization, N.A., A.E.A. and R.K.; Funding acquisition: M.F.A., J.K.A.-D. and A.S.A.-F.; Validation: A.S.A.-F. and R.K.; Resources, A.H.F. and A.S.A.-F.; Project Administration, A.S.A.-F., A.H.F. and A.E.A. All authors have read and agreed to the published version of the manuscript.

Funding: Researchers Supporting Project number (RSP2023R368), King Saud University, Riyadh, Saudi Arabia.

Data Availability Statement: There are no data to provide.

Acknowledgments: The authors would like to extend their sincere appreciation to Researchers Supporting Project number (RSP2023R368), King Saud University. R.K. and D.V. acknowledge Indus University for supporting research.

Conflicts of Interest: The authors declare no conflict of interest.

References

1. Quiroga, M.M.B.; Luna, A.E.C. Kinetic Analysis of Rate Data for Dry Reforming of Methane. *Ind. Eng. Chem. Res.* **2007**, *46*, 5265–5270. [CrossRef]
2. Al-Fatesh, A.S.; Patel, N.; Fakeeha, A.H.; Alotibi, M.F.; Alreshaidan, S.B.; Kumar, R. Reforming of Methane: Effects of Active Metals, Supports, and Promoters. *Catal. Rev. Sci. Eng.* **2023**, 1–99. [CrossRef]
3. Liao, M.-S.; Au, C.-T.; Ng, C.-F. Methane Dissociation on Ni, Pd, Pt and Cu Metal (111) a Theoretical Comparative Study. *Chem. Phy. Lett.* **1997**, *272*, 445–452. [CrossRef]
4. Liu, L.; Lin, Z.; Lin, S.; Chen, Y.; Zhang, L.; Chen, S.; Zhang, X.; Lin, J.; Zhang, Z.; Wan, S.; et al. Conversion of Syngas to Methanol and DME on Highly Selective Pd/$ZnAl_2O_4$ Catalyst. *J. Energy Chem.* **2021**, *58*, 564–572. [CrossRef]
5. Gallego, G.S.; Batiot-Dupeyrat, C.; Barrault, J.; Florez, E.; Mondragón, F. Dry Reforming of Methane over LaNi1-$YByO_{3\pm\delta}$ (B = Mg, Co) Perovskites Used as Catalyst Precursor. *Appl. Catal. A Gen.* **2008**, *334*, 251–258. [CrossRef]
6. Touahra, F.; Chebout, R.; Lerari, D.; Halliche, D.; Bachari, K. Role of the Nanoparticles of Cu-Co Alloy Derived from Perovskite in Dry Reforming of Methane. *Energy* **2019**, *171*, 465–474. [CrossRef]
7. Aramouni, N.A.K.; Zeaiter, J.; Kwapinski, W.; Leahy, J.J.; Ahmad, M.N. Trimetallic Ni-Co-Ru Catalyst for the Dry Reforming of Methane: Effect of the Ni/Co Ratio and the Calcination Temperature. *Fuel* **2021**, *300*, 120950. [CrossRef]
8. Erdogan, B.; Arbag, H.; Yasyerli, N. SBA-15 Supported Mesoporous Ni and Co Catalysts with High Coke Resistance for Dry Reforming of Methane. *Int. J. Hydrogen Energy* **2018**, *43*, 1396–1405. [CrossRef]
9. Li, S.; Zhang, G.; Wang, J.; Liu, J.; Lv, Y. Enhanced Activity of Co Catalysts Supported on Tungsten Carbide-Activated Carbon for CO_2 Reforming of CH_4 to Produce Syngas. *Int. J. Hydrogen Energy* **2021**, *46*, 28613–28625. [CrossRef]
10. Wu, Y.; Li, Y.; Gao, J.; Zhang, Q. Recent Advances in Vacancy Engineering of Metal-organic Frameworks and Their Derivatives for Electrocatalysis. *SusMat* **2021**, *1*, 66–87. [CrossRef]
11. Huang, H.; Yu, Y.; Zhang, M. Mechanistic Insight into Methane Dry Reforming over Cobalt: A Density Functional Theory Study. *Phys. Chem. Chem. Phys.* **2020**, *22*, 27320–27331. [CrossRef]
12. Jana, P.; De La Peña O'Shea, V.A.; Coronado, J.M.; Serrano, D.P. H_2 Production by CH_4 Decomposition over Metallic Cobalt Nanoparticles: Effect of the Catalyst Activation. *Appl. Catal. A Gen.* **2013**, *467*, 371–379. [CrossRef]
13. Zardin, L.; Perez-Lopez, O.W. Hydrogen Production by Methane Decomposition over Co-Al Mixed Oxides Derived from Hydrotalcites: Effect of the Catalyst Activation with H_2 or CH_4. *Int. J. Hydrogen Energy* **2017**, *42*, 7895–7907. [CrossRef]
14. Chen, S.; Zaffran, J.; Yang, B. Dry Reforming of Methane over the Cobalt Catalyst: Theoretical Insights into the Reaction Kinetics and Mechanism for Catalyst Deactivation. *Appl. Catal. B* **2020**, *270*, 118859. [CrossRef]
15. Gonzalez-Delacruz, V.M.; Pereñiguez, R.; Ternero, F.; Holgado, J.P.; Caballero, A. In Situ XAS Study of Synergic Effects on Ni-Co/ZrO_2 Methane Reforming Catalysts. *J. Phys. Chem. C* **2012**, *116*, 2919–2926. [CrossRef]
16. Al-Fatesh, A.; Singh, S.K.; Kanade, G.S.; Atia, H.; Fakeeha, A.H.; Ibrahim, A.A.; El-Toni, A.M.; Labhasetwar, N.K. Rh Promoted and ZrO_2/Al_2O_3 Supported Ni/Co Based Catalysts: High Activity for CO_2 Reforming, Steam–CO_2 Reforming and Oxy–CO_2 Reforming of CH4. *Int. J. Hydrogen Energy* **2018**, *43*, 12069–12080. [CrossRef]
17. Wu, Z.; Yang, B.; Miao, S.; Liu, W.; Xie, J.; Lee, S.; Pellin, M.J.; Xiao, D.; Su, D.; Ma, D. Lattice Strained Ni-Co Alloy as a High-Performance Catalyst for Catalytic Dry Reforming of Methane. *ACS Catal.* **2019**, *9*, 2693–2700. [CrossRef]
18. Luisetto, I.; Tuti, S.; Di Bartolomeo, E. Co and Ni Supported on CeO_2 as Selective Bimetallic Catalyst for Dry Reforming of Methane. *Int. J. Hydrogen Energy* **2012**, *37*, 15992–15999. [CrossRef]
19. Fan, M.S.; Abdullah, A.Z.; Bhatia, S. Utilization of Greenhouse Gases through Carbon Dioxide Reforming of Methane over Ni-Co/MgO-ZrO_2: Preparation, Characterization and Activity Studies. *Appl. Catal. B* **2010**, *100*, 365–377. [CrossRef]
20. Rahemi, N.; Haghighi, M.; Babaluo, A.A.; Jafari, M.F.; Khorram, S. Non-Thermal Plasma Assisted Synthesis and Physicochemical Characterizations of Co and Cu Doped Ni/Al_2O_3 Nanocatalysts Used for Dry Reforming of Methane. *Int. J. Hydrogen Energy* **2013**, *38*, 16048–16061. [CrossRef]
21. Sirois, S.; Castro, M.; Salahub, D.R. A Density Functional Study of the Interaction of CO_2 with a Pd Atom. *Int. J. Quantum Chem.* **1994**, *52*, 645–654. [CrossRef]
22. Jiménez, J.D.; Betancourt, L.E.; Danielis, M.; Zhang, H.; Zhang, F.; Orozco, I.; Xu, W.; Llorca, J.; Liu, P.; Trovarelli, A.; et al. Identification of Highly Selective Surface Pathways for Methane Dry Reforming Using Mechanochemical Synthesis of Pd-CeO_2. *ACS Catal.* **2022**, *12*, 12809–12822. [CrossRef] [PubMed]
23. Pan, C.; Guo, Z.; Dai, H.; Ren, R.; Chu, W. Anti-Sintering Mesoporous Ni–Pd Bimetallic Catalysts for Hydrogen Production via Dry Reforming of Methane. *Int. J. Hydrogen Energy* **2020**, *45*, 16133–16143. [CrossRef]
24. Steinhauer, B.; Kasireddy, M.R.; Radnik, J.; Martin, A. Development of Ni-Pd Bimetallic Catalysts for the Utilization of Carbon Dioxide and Methane by Dry Reforming. *Appl. Catal. A Gen.* **2009**, *366*, 333–341. [CrossRef]

25. Zambaldi, P.; Haug, L.; Penner, S.; Klötzer, B. Dry Reforming of Methane on NiCu and NiPd Model Systems: Optimization of Carbon Chemistry. *Catalysts* **2022**, *12*, 311. [CrossRef]
26. Ahn, S.H.; Klein, M.J.; Manthiram, A. 1D Co- and N-Doped Hierarchically Porous Carbon Nanotubes Derived from Bimetallic Metal Organic Framework for Efficient Oxygen and Tri-Iodide Reduction Reactions. *Adv. Energy Mater.* **2017**, *7*, 1601979. [CrossRef]
27. Al-Fatesh, A.S.; Chaudhary, M.L.; Fakeeha, A.H.; Ibrahim, A.A.; Al-Mubaddel, F.; Kasim, S.O.; Albaqmaa, Y.A.; Bagabas, A.A.; Patel, R.; Kumar, R. Role of Mixed Oxides in Hydrogen Production through the Dry Reforming of Methane over Nickel Catalysts Supported on Modified γ-Al_2O_3. *Processes* **2021**, *9*, 157. [CrossRef]
28. Hassan, S.; Kumar, R.; Tiwari, A.; Song, W.; van Haandel, L.; Pandey, J.K.; Hensen, E.; Chowdhury, B. Role of Oxygen Vacancy in Cobalt Doped Ceria Catalyst for Styrene Epoxidation Using Molecular Oxygen. *Mol. Catal.* **2018**, *451*, 238–246. [CrossRef]
29. Tang, Q.; Zhang, Q.; Wu, H.; Wang, Y. Epoxidation of Styrene with Molecular Oxygen Catalyzed by Cobalt(II)-Containing Molecular Sieves. *J. Catal.* **2005**, *230*, 384–397. [CrossRef]
30. Luo, M.-F.; Hou, Z.-Y.; Yuan, X.-X.; Zheng, X.-M. Characterization Study of CeO_2 Supported Pd Catalyst for Low-Temperature Carbon Monoxide Oxidation. *Catal. Lett.* **1998**, *50*, 205–209. [CrossRef]
31. Patel, R.; Al-Fatesh, A.S.; Fakeeha, A.H.; Arafat, Y.; Kasim, S.O.; Ibrahim, A.A.; Al-Zahrani, S.A.; Abasaeed, A.E.; Srivastava, V.K.; Kumar, R. Impact of Ceria over WO_3–ZrO_2 Supported Ni Catalyst towards Hydrogen Production through Dry Reforming of Methane. *Int. J. Hydrogen Energy* **2021**, *46*, 25015–25028. [CrossRef]
32. Pan, Q.; Peng, J.; Sun, T.; Wang, S.; Wang, S. Insight into the Reaction Route of CO_2 Methanation: Promotion Effect of Medium Basic Sites. *Catal. Commun.* **2014**, *45*, 74–78. [CrossRef]
33. Al-Fatesh, A.S.; Patel, N.; Srivastava, V.; Osman, A.I.; Rooney, D.W.; Fakeeha, A.H.; Abasaeed, A.E.; Alotibi, M.F.; Kumar, R. Iron-Promoted Zirconia-Alumina Supported Ni Catalyst for Highly Efficient and Cost-Effective Hydrogen Production via Dry Reforming of Methane. *J. Environ. Sci.* **2023**. [CrossRef]
34. Abasaeed, A.E.; Lanre, M.S.; Kasim, S.O.; Ibrahim, A.A.; Osman, A.I.; Fakeeha, A.H.; Alkhalifa, A.; Arasheed, R.; Albaqi, F.; Kumar, N.S.; et al. Syngas Production from Methane Dry Reforming via Optimization of Tungsten Trioxide-Promoted Mesoporous γ-Alumina Supported Nickel Catalyst. *Int. J. Hydrogen Energy* **2022**, *48*, 26492–26505. [CrossRef]
35. Li, R.; Jin, B.; Ma, T.; Liang, Y.; Wei, Y.; Yu, X.; Li, J.; Liu, J.; Zhao, Z. Highly Efficient Catalysts of AuPd Alloy Nanoparticles Supported on 3D Ordered Macroporous Al_2O_3 for Soot Combustion. *ChemCatChem* **2022**, *14*, e202201020. [CrossRef]
36. Ferrari, A.C.; Robertson, J. Resonant Raman Spectroscopy of Disordered, Amorphous, and Diamondlike Carbon. *Phys. Rev. B Condens. Matter Mater. Phys.* **2001**, 64. [CrossRef]
37. Charisiou, N.D.; Tzounis, L.; Sebastian, V.; Hinder, S.J.; Baker, M.A.; Polychronopoulou, K.; Goula, M.A. Investigating the Correlation between Deactivation and the Carbon Deposited on the Surface of Ni/Al_2O_3 and Ni/La_2O_3-Al_2O_3 Catalysts during the Biogas Reforming Reaction. *Appl. Surf. Sci.* **2019**, *474*, 42–56. [CrossRef]
38. Kim, H.; Robertson, A.W.; Kwon, G.H.; Jang-Won, O.; Warner, J.H.; Kim, J.M. Biomass-Derived Nickel Phosphide Nanoparticles as a Robust Catalyst for Hydrogen Production by Catalytic Decomposition of C_2H_2 or Dry Reforming of CH_4. *ACS Appl. Energy Mater.* **2019**, *2*, 8649–8658. [CrossRef]
39. Li, X.; Chang, J.-S.; Tian, M.; Park, S.-E. CO_2 Reforming of Methane over Modi®ed Ni/ZrO_2 Catalysts. *Appl. Organomet. Chem.* **2001**, *15*, 109–112. [CrossRef]
40. Kambolis, A.; Matralis, H.; Trovarelli, A.; Papadopoulou, C. Ni/CeO_2-ZrO_2 Catalysts for the Dry Reforming of Methane. *Appl. Catal. A Gen.* **2010**, *377*, 16–26. [CrossRef]
41. Charisiou, N.D.; Siakavelas, G.; Tzounis, L.; Sebastian, V.; Monzon, A.; Baker, M.A.; Hinder, S.J.; Polychronopoulou, K.; Yentekakis, I.V.; Goula, M.A. An in Depth Investigation of Deactivation through Carbon Formation during the Biogas Dry Reforming Reaction for Ni Supported on Modified with CeO_2 and La_2O_3 Zirconia Catalysts. *Int. J. Hydrogen Energy* **2018**, *43*, 18955–18976. [CrossRef]
42. Mourhly, A.; Kacimi, M.; Halim, M.; Arsalane, S. New Low Cost Mesoporous Silica (MSN) as a Promising Support of Ni-Catalysts for High-Hydrogen Generation via Dry Reforming of Methane (DRM). *Int. J. Hydrogen Energy* **2020**, *45*, 11449–11459. [CrossRef]
43. Titus, J.; Goepel, M.; Schunk, S.A.; Wilde, N.; Gläser, R. The Role of Acid/Base Properties in Ni/MgO-ZrO_2–Based Catalysts for Dry Reforming of Methane. *Catal. Commun.* **2017**, *100*, 76–80. [CrossRef]
44. Kurdi, A.N.; Ibrahim, A.A.; Al-Fatesh, A.S.; Alquraini, A.A.; Abasaeed, A.E.; Fakeeha, A.H. Hydrogen Production from CO_2 Reforming of Methane Using Zirconia Supported Nickel Catalyst. *RSC Adv.* **2022**, *12*, 10846–10854. [CrossRef]
45. Liang, T.Y.; Lin, C.Y.; Chou, F.C.; Wang, M.; Tsai, D.H. Gas-Phase Synthesis of Ni-CeO_x Hybrid Nanoparticles and Their Synergistic Catalysis for Simultaneous Reforming of Methane and Carbon Dioxide to Syngas. *J. Phys. Chem. C* **2018**, *122*, 11789–11796. [CrossRef]